THE PLANCK-SHANNON PLOT: A QUANTITATIVE METHOD FOR IDENTIFYING 'SUPERSTRUCTURES' IN CELL BIOLOGY AND CONSCIOUSNESS STUDY

Sungchul Ji

ABSTRACT: The recently (1997-2019) developed cell language theory predicts the existence of 'superstructures' including supermetabolic pathways and 'superneural networks'. The present paper describes how the Planckian Distribution Equation discovered in 2008 and its derivative, the Planck-Shannon plot, might be utilized to quantitate the state of human consciousness (or to measure the 'quanta of consciousness') based on multichannel EEG data properly transformed into long tailed histograms.

KEYWORDS: Superstructures; Cell language theory; Blackbody radiation equation; Planckian Distribution Equation; Planckian information of the second kind; Planck-Shannon plot; Superneural networks and consciousness; Quantum of consciousness; Quantitative consciousness studies

INTRODUCTION

According to the cell language theory formulated in 1997 [1, 2, 3], living cells communicate with one another using a molecular language called 'cellese'. In [3]. it was postulated that there were4 distinct levels of organization in cellese as well as in human language (*humanese*), the four levels being *letters*, *words*, *sentences,* and *texts* (see **Table 4** in [3]). However, the 4-level structure was subsequently modified into a 5-level structure shown in **Table** 1 below in order to fit better the quantitative regularities found in long nucleotide sequences in DNA [4] and the Multiple Codes of Nucleotides Sequences (MCNS) hypothesis of Trifonov [5, 6]. The MCNS hypothesis states that:

"*Nucleotide sequences carry genetic information of many different kinds, not just instructions for protein synthesis (triplet code). Several codes of nucleotide sequences are discussed including:*

(1) the translation framing code, responsible for correct triplet counting by the ribosome during protein synthesis; (2) the chromatin code, which provides instructions on appropriate placement of nucleosomes along the DNA molecules and their spatial arrangement; (3) a putative loop code for single-stranded RNA-protein interactions. The codes are degenerate and corresponding messages are not only interspersed but actually overlap, so that some nucleotides belong to several messages simultaneously. Tandemly repeated sequences frequently considered as functionless "junk" are found to be grouped into certain classes of repeat unit lengths. This indicates some functional involvement of these sequences. A hypothesis is formulated according to which the tandem repeats are given the role of weak enhancer-silencers that modulate, in a copy number-dependent way, the expression of proximal genes. Fast amplification and elimination of the repeats provides an attractive mechanism of species adaptation to a rapidly changing environment."

To the best of my knowledge, this statement (which may be referred to as the *Trifonov hypothesis* or the *MCNS hypothesis*) has largely been validated by the numerous findings reported in the molecular and cellular genetics literature during the past three decades.

Table 1. Five levels of the information (or organization) in DNA (*Cellese*) and the human language (*Humanese*): A hypothesis.

Organization	DNA (Cellese)	Human Language (Humanese)
1st Level (To Build)	Nucleotides ---> 1-D n-Plets[1]	Letters ---> Phonemes[2]
2nd Level (To Differ)	1-D n-Plets ---> 1-D Structures (Encoding primary structures of genes)	Phonemes ---> Sememes[3]
3rd Level (To Denote)	1-D Structures ---> 3-D Structures[4]	Sememes ---> Words

	(Encoding not only the amino acid sequences of enzymes but also their copy numbers)	
4th Level (To Decide)	3-D Structures ---> 4-D Structures[5] (Encoding metabolic pathways)	Words --- > Sentences
5th Level (To Compute/Reason)	4-D Structures ---> 5-D Structures[6] (super-metabolic pathways)	Sentences ---> Algorithms/Syllogism

[1] Sets of n nucleotides linked linearly through covalent bonds, where n = 1, 2, 3, . . . , 10^6 (?).
[2] Units of sounds the human vocal system can generate.
[3] Units of meaning
[4] The DNA molecules folded in the 3-D space are thought to constitute both the structural genes encoding not only the usual amino acid sequences but also the 'spatiotemporal' genes [12, pp. 177-178] that are postulated to regulate the copy number of a gene under a given cellular environment.
[5] The DNA molecule whose 4-D structure is such that it executes a time-dependent, programmed structural changes upon being excited by free energy input through ligand binding or energy input catalyzed by enzymes.
[6] The DNA molecule whose 3-D structure is such that it encodes not only metabolic pathways individually but also their mutual interactions so as to accomplish a common cellular function such aa chemotaxis.

Of the five levels of organization, this paper will focus on the last three levels, i.e., *enzymes*, *metabolic pathways*, and *systems of two or more metabolic pathways* that are coupled or cooperate to accomplish some cell functions. Such higher-order metabolic pathways are referred to as "*superstructures*" or "*supermetabolic pathways*'

which are closely related to what Norris called 'hyperstructures' in 1999 [7].

The purpose of this paper is two-fold – (i) To describe the Planck-Shannon Plot (PSP) rooted in the Planckian Distribution Equation (PDE) discovered at Rutgers in 2008 [8], and (ii) To apply PSP to quantifying consciousness viewed as a superstructure or superneural network in the human brain based on EEG data.

PLANCKIAN DISTRIBUTION EQUATION (PDE) AND ITS DERIVATION FROM THE BLACKBODY RADIATION EQUATION (BRE)

In 2008 I noticed that the long-tailed histogram of the single-molecule enzyme turnover times reported by Lu et al [9] resembled the blackbody radiation spectrum at 6000 °K (compare **Figures 1b** and **1d**). This observation motivated me to generalize the blackbody radiation equation (BRE) of Max Planck (1858-1947), Eq. (1) in **Figure 2a**, by replacing its universal constants and temperature with free parameters, A, B and C, resulting in the so-called Planckian Distribution Equation (PDE), Eq. (2), shown in **Figure 2b**. Eq. (2) was later simplified as Eq. (3)**, Figure 2c.** Eqs. (2) and (3) are interconvertible through Eqs. (4), (5), and (6) [10]. It is often more convenient to use Eq. (2) than Eq. (3) to fit certain long-tailed histograms.

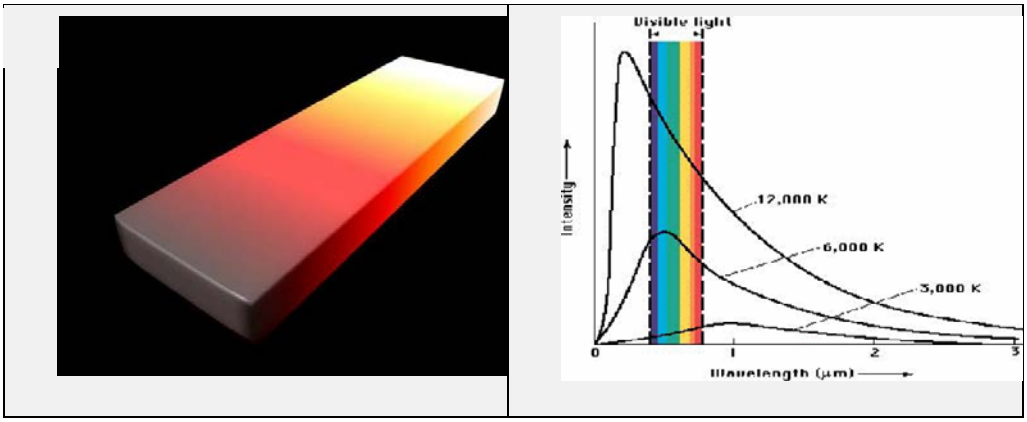

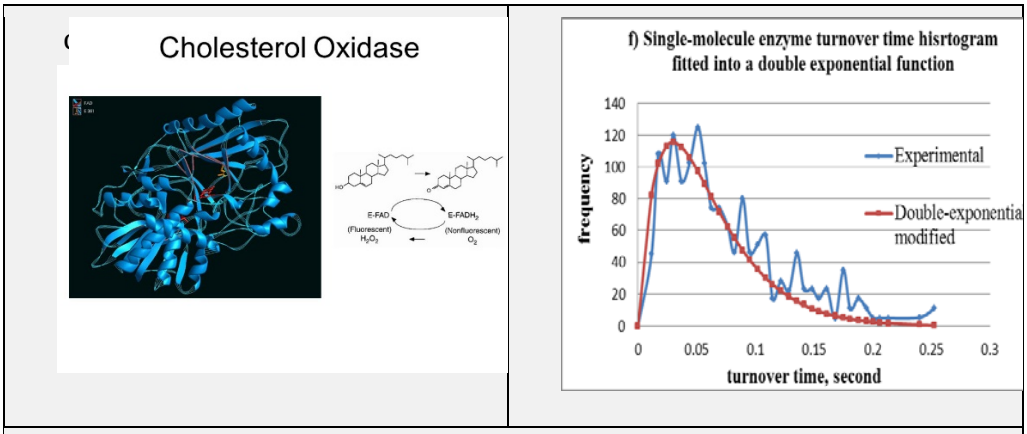

Figure 1. Isomorphism between the blackbody radiation and single-molecule enzyme catalysis. (**a**) Blackbody radiation. (**b**) Blackbody radiation spectra. (**c**) The 3-D structure of cholesterol oxidase. (**d**) The histogram of the cholesterol oxidase enzyme turnover times.

Evidently, PDE, i.e., Eq. (2) or Eq. (3), is isomorphic with BRE, Eq. (1), in mathematical form. The blackbody radiation equation (BRE), Eq. (1), is the product of two terms, the first term, $(2\pi hc^2/\lambda^5)$, being related to the number of the mode of vibrations per unit frequency and unit volume, and the second term, $1/(e^{hc/\lambda kT} - 1)$, to the average energy per mode [11]. Since PDE is mathematically isomorphic with BRE, it seems reasonable to postulate that the two terms in PDE, Eq. (2), have the same physical meanings as in Eq. (1) (see **Figure 2b**).

(

$$E(\lambda, T) = \frac{2\pi hc^2}{\lambda^5 (e^{\frac{hc}{\lambda kT}} - 1)}$$

(1)

λ = Wavelength c = Speed of light

k = Boltzmann constant

h = Planck's constant

e = 2.71828182

[T] = Kelvin (Temperature)

[λ] = Meters

h = 6.626.1034 J.s

c = 2.998.108 m/s

k = 1.381.10-23 J/K

(

$$y = \frac{a}{(Ax + B)^5} \quad \frac{1}{e^{b/(Ax+B)} - 1} \qquad (2)$$

Number of modes of vibrations per unit frequency per unit volume

Average energy per mode

(

$$y = \frac{A}{(x + B)^5} \cdot \frac{1}{e^{C/(x+B)} - 1} \qquad (3)$$

$$A = a/A^5 \qquad (4)$$

	B = B/A (5) **C = b/A** (6)

Figure 2. The relation between the Planckian Distribution Equation (PDE) and the blackbody radiation equation (BRE). Adopted from [1, **Figure 8.1**]. (**a**) The Planck radiation equation. Reproduced from [11]. (**b**) The 4-parameter Planckian Distribution Equation, also called the blackbody radiation-like equation (BRE) or the generalized Planck equation (GPE) [1, Chapter 8]. (**c**) The 3-parameter (colored red) version of PDE. The relations between the 4- and 3-parameter versions of PDE are given in Eqs. (4), (5), and (6).

As evident in **Figure 1d**, the single-molecule enzyme kinetic data fit PDE. It was later found that PDE can fit almost any long-tailed histograms examined so far. Twenty examples of long tailed histograms fitting PDE are given in **Figure 8.6** in [1], and these histograms were reported from various fields, including atomic physics, protein folding, single-molecule enzymology, whole-cell RNA metabolism (see **Figure 3** below), glottometrics (i.e., the quantitative study of languages and texts), ECoG (electrocorticography), fMRI (functional Magnetic Resonance Imaging), psychophysics, econometrics, and Big Bang cosmology [1, **Figure 8.6**].

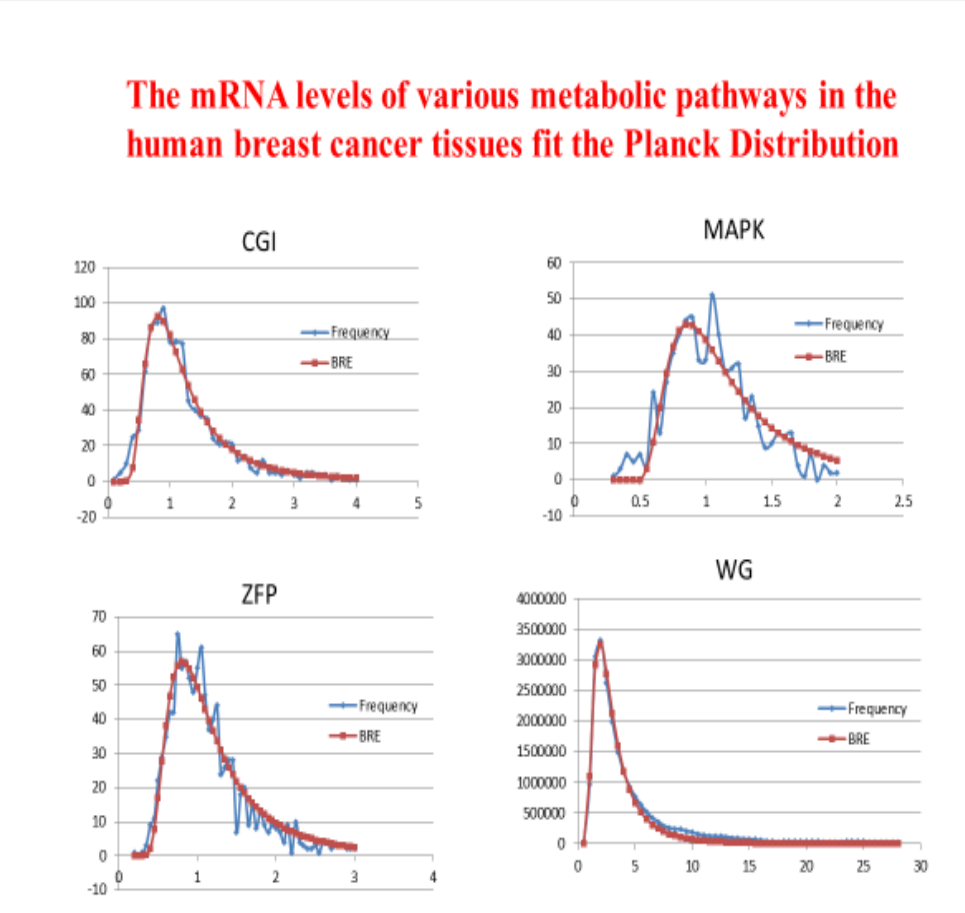

Figure 3. Some examples of long-tailed histograms (blue curves; mRNA levels of genes encoding various metabolic pathways in human breast tissues) fitting PDE (red curves), also called Planckian Distribution. BRE = Blackbody Radiation-like Equation, synonymous with PDE, Planckian Distribution Equation. CGI = tissue binding proteins; MAPK = mitogen-activated protein kinase; ZFP = zinc finger protein; WG = whole genome. Reproduced from **Figure 7.16** in [1].

One possible explanation for the apparent universality of PDE can be provided based on the interpretation of PDE given in **Figure 2b:**

(i) Whenever physicochemical processes generate numerical data representable as long-tailed histograms fitting PDE, those processes (referred to as *Planckian processes*, or *Planckons* in [3]) may implicate wave phenomena, because

the first factor in PDE is related to the number of vibrational modes per unit frequency per unit volume of the system under consideration and vibrational/oscillatory motions may be said to underlie wave motions at all physical scales from the microscopic to the mesoscopic and to the macroscopic.

(ii) The measurable properties of all the physicochemical systems performing Planckian processes are determined by the standing waves generated within the system, similar to the musical melodies being determined by the standing waves generated within musical instruments. A similar conclusion was reached by Petoukhov that all organisms are akin to musical instruments based on his quantitative analysis of the long DNA sequences using the same mathematical tools employed by engineers in analyzing mechanical waves [4].

(iii) These ideas are schematically summarized in **Figure 4.**

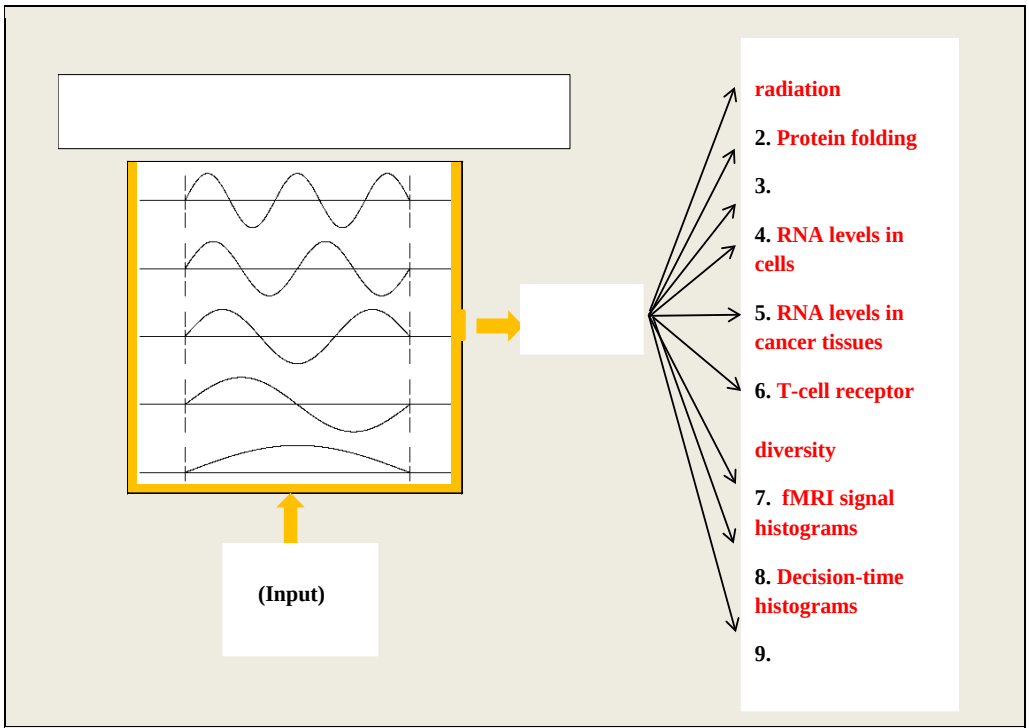

Figure 4. One possibility to account for the universality of the Planckian distribution in nature is to postulate that the *wave-particle duality* first discovered in atomic physics in the early 20th century operates at all scales of material systems, from atoms to enzymes to cells to brains and to the Universe Itself. Reproduced from [1, **Figure 8.8**].

PLANCKIAN DISTRIBUTION EQUATION (PDE) AND ITS DERIVATION FROM THE GAUSSIAN DISTRIBUTION EQUATION (GDE)

As evident in **Figure 5** (**b**), the rising phase of PDE more or less overlaps with the rising phase of a Gaussian-like equation (GLE), Eq. (7). GLE was derived from the Gaussian distribution equation by replacing its pre-exponential factor with a free parameter, A:

$$y = Ae^{-(x-\mu)^2/(2\sigma^2)} \qquad (7)$$

It was found that GDE and PDE can be quantitatively related based on the drift-diffusion model (DDM) of decision making [1, **Figure 8.7**]. DDM of decision making is widely employed in modelling the behavioral neurobiological phenomenon. When a person is presented with a problem to be solved with a binary decision, the more difficult the problem is, the longer it takes for the person to come to a decision [13, 14, 15, 16, 17]. Although not shown here, DDM accurately reproduces the decision-time histograms (see the blue curve in **Figure 5b** below), which can be reproduced almost exactly by PDE (see the red curve in **Figure 8.6** (q) in [1]).

Figure 3a depicts two essential features of DDM: (i) The Gaussian-distributed *drift rates* (i.e., the rates of evidence accumulation in the brain), which can be represented as tan α, where α is the arctangent of the drift rate, D/t, with D being the decision threshold and t the decision time, and (ii) the nonlinear relation between the independent variable of the Gaussian distribution and the decision times.

Because of these two features, the Gaussian-distributed drift rates can produce a right-long tailed decision-time histogram fitting PDE (see **Figures 3a and c**).

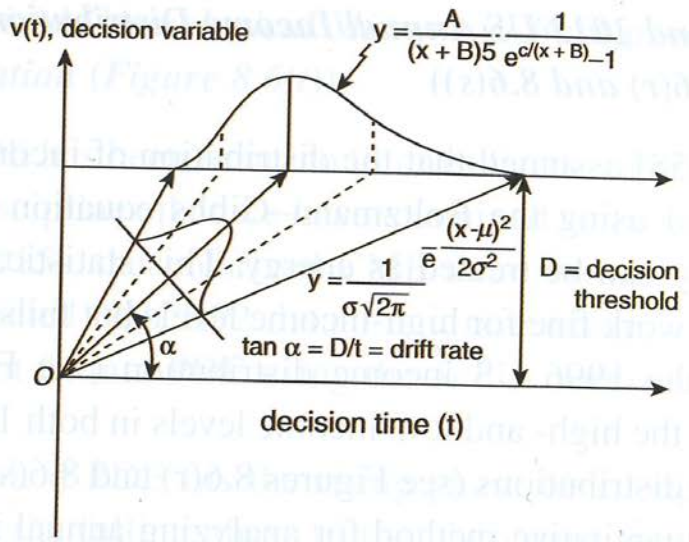

(a)

The Gaussian component of the decision-time distribution

Data from G. Deco, E. T. Rolls, *et al.* (2013). *Progr. Neurobiol.* **103**:194-213;
Fig. 2b. μ = 120, σ = 50. S. Ji, 5/8/2014

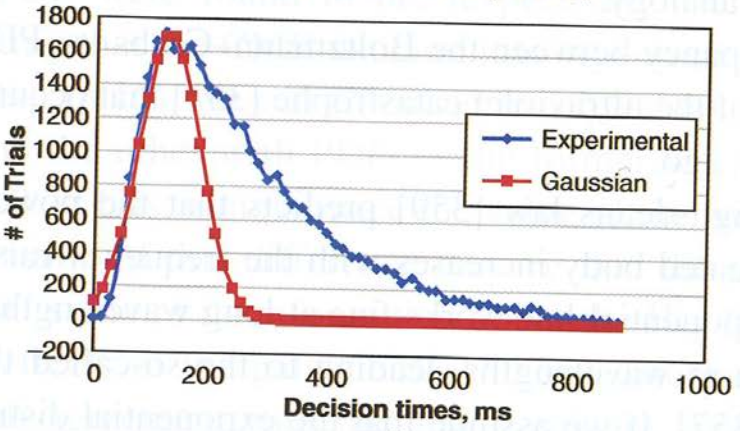

(b)

The Gaussian distribution transformed by the rule x=> D/tan x becomes a Planckian distribution !

A = 32, B = –1, C = 40, RMAD = 56.676, by trial & error fitting S. Ji, 6/13/2014

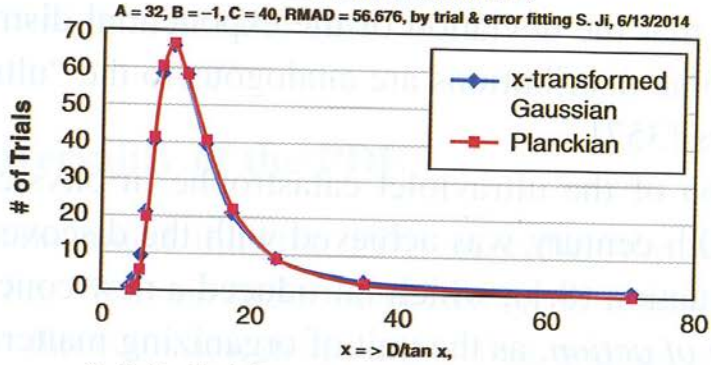

S = Decision threshold, and x is the arc tan of drift rate μ. i.e., D/decision time.

(c)

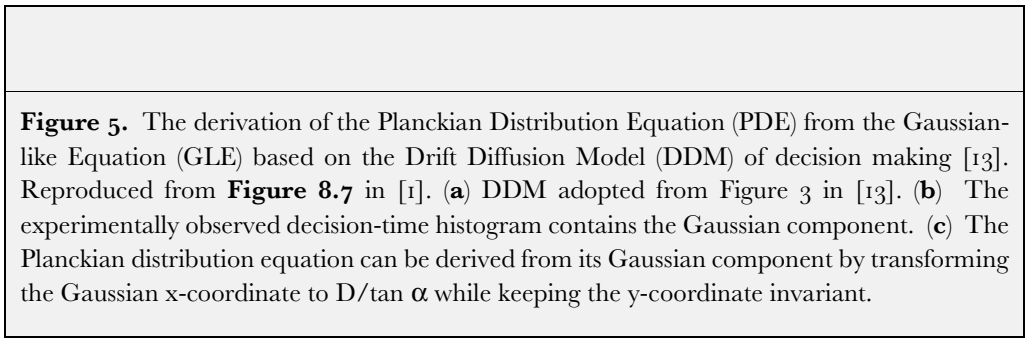

Figure 5. The derivation of the Planckian Distribution Equation (PDE) from the Gaussian-like Equation (GLE) based on the Drift Diffusion Model (DDM) of decision making [13]. Reproduced from **Figure 8.7** in [1]. (**a**) DDM adopted from Figure 3 in [13]. (**b**) The experimentally observed decision-time histogram contains the Gaussian component. (**c**) The Planckian distribution equation can be derived from its Gaussian component by transforming the Gaussian x-coordinate to D/tan α while keeping the y-coordinate invariant.

The results shown in **Figure 5a** and **c** demonstrate that Planckian processes can result from Gaussian processes given appropriate selection mechanisms as diagrammatically shown in **Figure 6.**

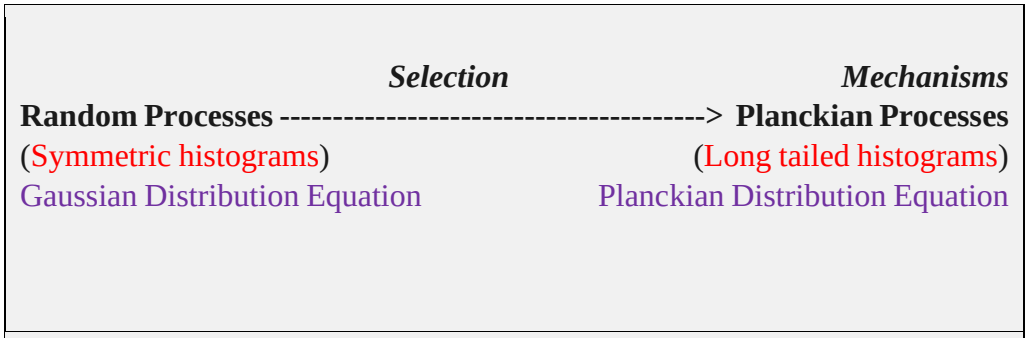

Figure 6 A diagrammatic definition of the Planckian processes (PP), or Planckons, as the subset of random processes selected through some generative mechanisms. Random processes are characterized by symmetric distributions obeying the Gaussian distribution equation while Planckian processes are characterized by asymmetric long-tailed histograms fitting PDE [10].

PLANCKIAN INFORMATION OF THE SECOND KIND, SHANNON ENTROPY, AND PDE

Once PDE is found to fit a long-tailed histogram, two numbers can be computed from it – (i) the Planckian information of the second kind (I_{PS}), and (ii) Shannon entropy (H) as previously described [18], which allows the construction of the so-called Planck-Shannon plot [18] (see **Figure 7** below):

$$I_{PS} = - \log_2 ((\mu - mode)/\sigma) \quad (8)$$

(1)

where μ and σ are the mean and the standard deviation of the long-tailed histogram under consideration.

$$H = -\Sigma\, p_i \log_2 p_i \quad (9)$$

where p_i is the probability of observing the i^{th} event.

PLANCK-SHANNON PLOTS AS A SUPERSTRUCTURES-IDENTIFIER (SSI)

"Structure" is here defined as any set of elements whose numerical values can be represented as a long-tailed histogram fitting PDE. "Superstructure" is defined as a set of correlated structures. For example, the metabolic pathway transforming glucose to pyruvate (called the glycolytic pathway) implicating about a dozen enzymes is a structure since the intracellular levels of the mRNA molecules synthesized by these enzymes produce a long-tailed histogram that fits PDE.

We analyzed 10 metabolic pathways (including CGI protein, DKFZP protein, KIAA protein, ribosomal protein, zinc finger protein, etc, each encoded by about 50 genes) measured by Perou et al from 20 breast cancer patients before and after treating with doxorubicin for 16 week [19]. Four examples of the mRNA histograms (blue curves) fitting PDE (red curves) are displayed in **Figure 3**. Five examples of the Planck-Shannon plots of the mRNA levels measured from human breast cancer tissues before and after treating with the anticancer drug, doxorubicin, are shown in **Figure 7**.

	Before Drug Treatment	After Drug Treatment

P 2 (30; 9)	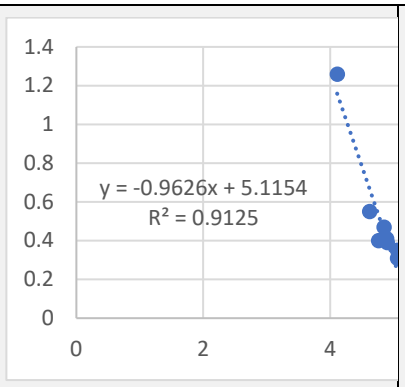	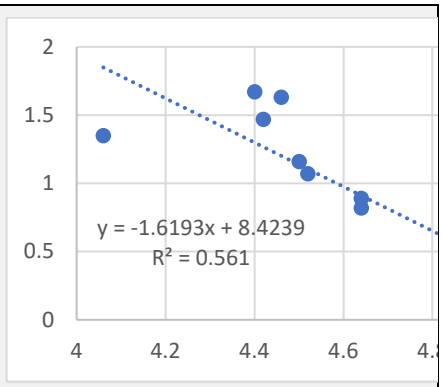
P 5 (79; 10)	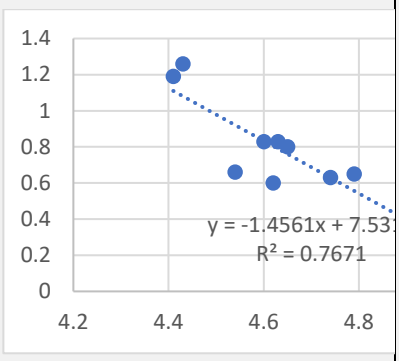	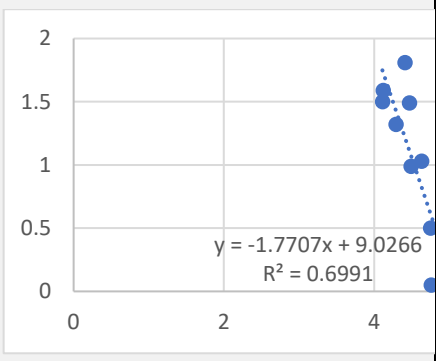
P 11 (66; 10)	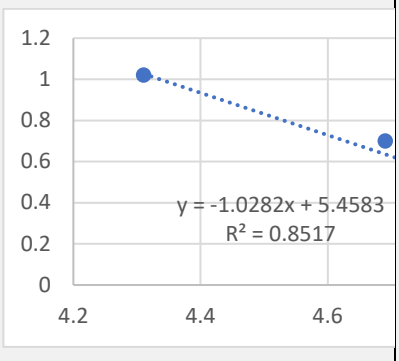	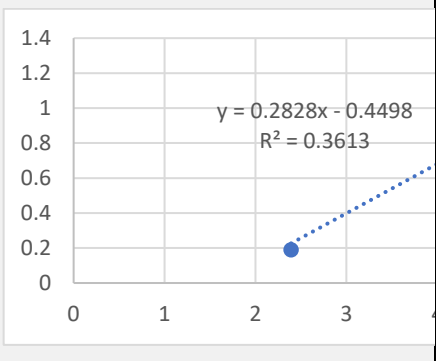

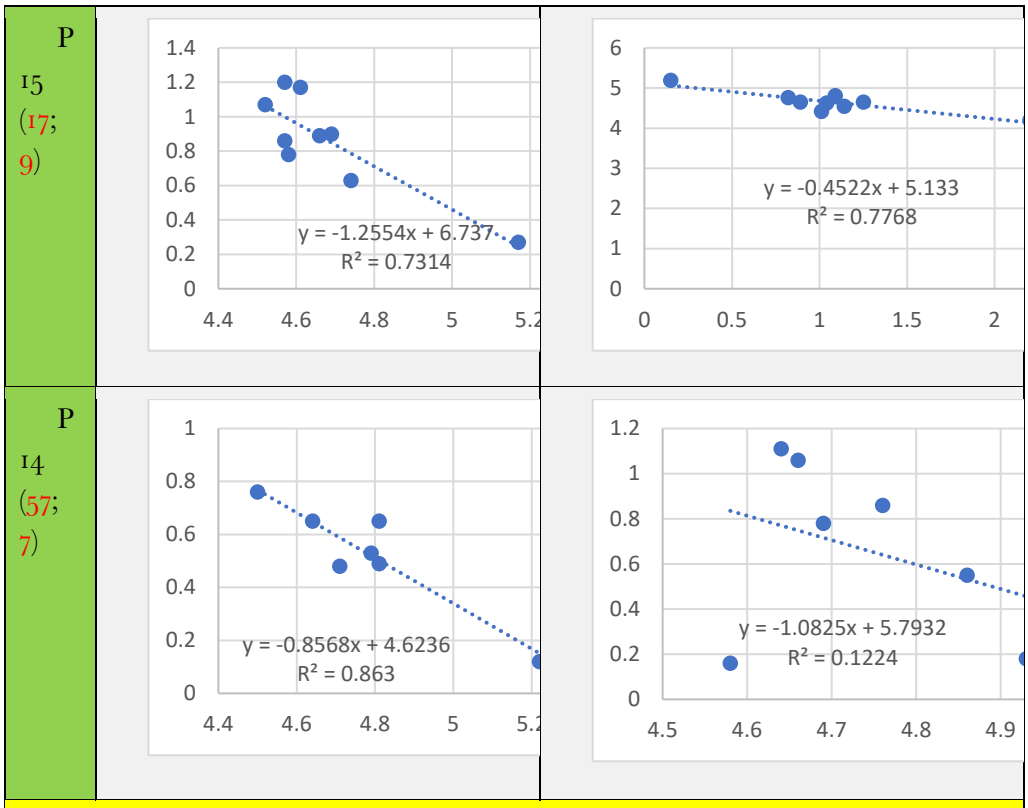

Figure 7. The *Planck-Shannon plots* of 7-10 metabolic pathways (for each histogram) before and after treating with doxorubicin. Patient # (survival months; number of pathways in the plot). The x-axis encodes the Shannon entropy, H, and the y-axis encodes the Planckian information of the second kind, $\mathbf{I}_{\mathbf{PS}}$, [18].

Over the last several years, my students at Ernest Mario School of Pharmacy (EMSP) at Rutgers and I have found quantitative evidence that the anticancer drug, doxorubicin, works by affecting patient-specific sets of metabolic pathways (each consisting of about a dozen enzymes) and supermetabolic pathways (each consisting of 2 to 10 metabolic pathways). The results are summarized in **Figure 8**.

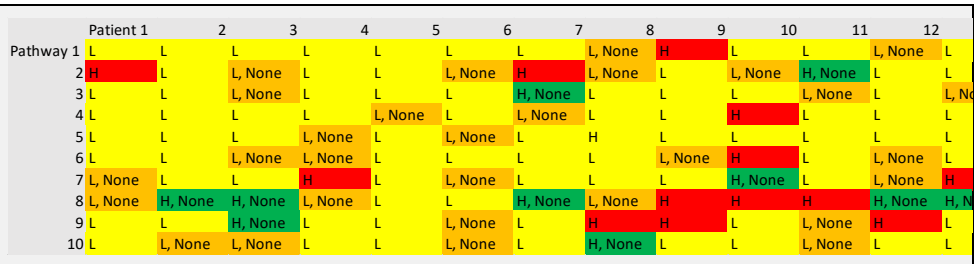

	Patient 1	2	3	4	5	6	7	8	9	10	11	12	
Pathway 1	L	L	L	L	L	L	L	L, None	H	L	L	L, None	L
2	H	L	L, None	L	L	L, None	H	L, None	L	L, None	H, None	L	L
3	L	L	L, None	L	L	L	H, None	L	L	L	L, None	L	L, N
4	L	L	L	L	L, None	L	L, None	L	L	H	L	L	L
5	L	L	L	L, None	L	L, None	L	H	L	L	L	L	L
6	L	L	L, None	L, None	L	L	L	L	L, None	H	L	L, None	L
7	L, None	L	L	H	L	L, None	L	L	L	H, None	L	L, None	H
8	L, None	H, None	H, None	L, None	L	L	H, None	L, None	H	H	H	H, None	H, N
9	L	L	H, None	L	L	L, None	L	H	H	L	L, None	H	L
10	L	L, None	L, None	L	L	L, None	L	H, None	L	L	L, None	L	L

Figure 8. Patient-specific, doxorubicin-sensitive metabolic pathways identified with the Planck-Shannon plot.

H = Hight sensitivity to doxorubicin (based on the Planck-Shannon plot) (26)

L = Low sensitivity to doxorubicin (based on the Planck-Shannon plot) (124)

None = No sensitivity to doxorubicin (based on the Planck-Shannon plot) (46)

The key points of **Figure 8** are:

(1) The rows indicate metabolic pathways (1 through 10), and the columns indicate patients (1 through 15).

(2) Drug responses are divided into three levels -- high (H), low (L), and none (N). Two methods were used to measure the drug responses, i.e., the Planck-Shannon plot as shown in **Figure 7** and the changes in the C/A ratio of PDE (less than 30% change in this ratio induced by doxorubicin being considered as non-responding).

(3) There is no metabolic pathway that responded to doxorubicin in the same way in all 15 patients. That is, there are no rows that are coloured uniformly.

(4) There are no patients that responded to doxorubicin in the same way. That is, there are no columns whose colour patterns are identical.

(5) Findings (3) and (4) demonstrate that

"The drug effect is not only patient specific but also metabolic-pathway specific in a given patient."

For convenience of future discussion, this finding will be referred to as the "**P**atient and **M**etabolic **P**athway **S**pecific **D**rug **E**ffects" (PMSDE).

It should be noted that, if the PDE-based classification method is 100%

accurate, there should be no boxes that contain both H and N; but there are 11 of these out of 150. So, the accuracy of this method may be estimated to be (11/150)x100 = 7.3% or about 8%.

As can be seen in **Figure 7**, most of the Planck-Shannon plots constructed from the mRNA data associated with 10 metabolic pathways measured from 15 human breast cancer tissues, either before or after drug treatment, showed good liner correlations with R^2 values greater than 0.6. This indicates that these metabolic pathways are coupled to carry out some cell functions (e.g., cellular reasoning or computations underlying morphogenesis, wound healing, immune response, etc.) and hence constitute "supermetabolic pathways" as defined at the beginning of this section. Supermetabolic pathways can be readily identified in Planck-Shannon plots since they appear as *a set of points that are linearly correlated*. Any point on a Planck-Shannon plot qualifies as a structure as defined above, regardless of whether or not it constitutes a component of a linear regression line. Thus the Planck-Shannon plot provides a convenient visual (qualitative) and quantitative method for distinguishing between "structures" (points on the PSP) and "superstructures" (lines or linear clusters of points on the PSP). Since all of the superstructures shown in **Figure 7** are sensitive to drug treatment (as indicated by changes in the slopes or R^2 values), they constitute what may be referred to as "druggable superstructures" or "druggable supermetabolic pathways" [18]. The drug-responsivity or -sensitivity of supermetabolic pathways can be estimated in terms of drug-induced changes in the slopes or the correlation coefficients of the linear regression lines in the Planck-Shannon plots. Thus, it is clear that the Planck-Shannon plot can be employed as a quantitative tool for discovering drugs for various diseases.

POTENTIAL APPLICATIONS OF PDE TO THE QUANTITATIVE STUDY OF CONSCIOUSNESS: TOWARD THE QUANTITATIVE CONSCIOUSNESS STUDY (QCS).

The Planck Distribution Equation (PDE) and the Planck-Shannon plots (PSP) can be applied to discovering superstructures in any fields as long as they generate long-tailed histograms. Since EEG signals measured with multichannel EEG devices (see **Figures 9a** and **9b**) and transformed properly also generate long-tailed histograms (see **Figures 9c** and **9d**), it can be predicted that PDE and PSP

should be applicable to discovering the superstructures (associated with specific mental states or tasks ?) in the human brains. More specifically, PDE and PSP may allow neuroscientists to identify the brain regions associated with *consciousness* as well as the brain superstructures that are brain region- and mental task-specific, generating results similar to those shown in **Figure 8,** with the names of the row and the column replaced with *brain tasks* and *brain regions*, respectively. Further details of my predictions are briefly summarized in the legend to **Figure 9**.

a	b
	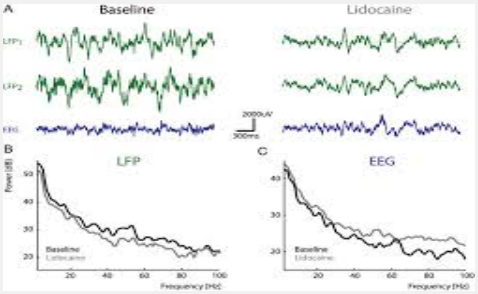
http://www.gtec.at/Products/Hardware-and-Accessories/	https://pdfs.semanticscholar.org/8769/b68a15d7f766c4cf888928a4241694c4367a.pdf

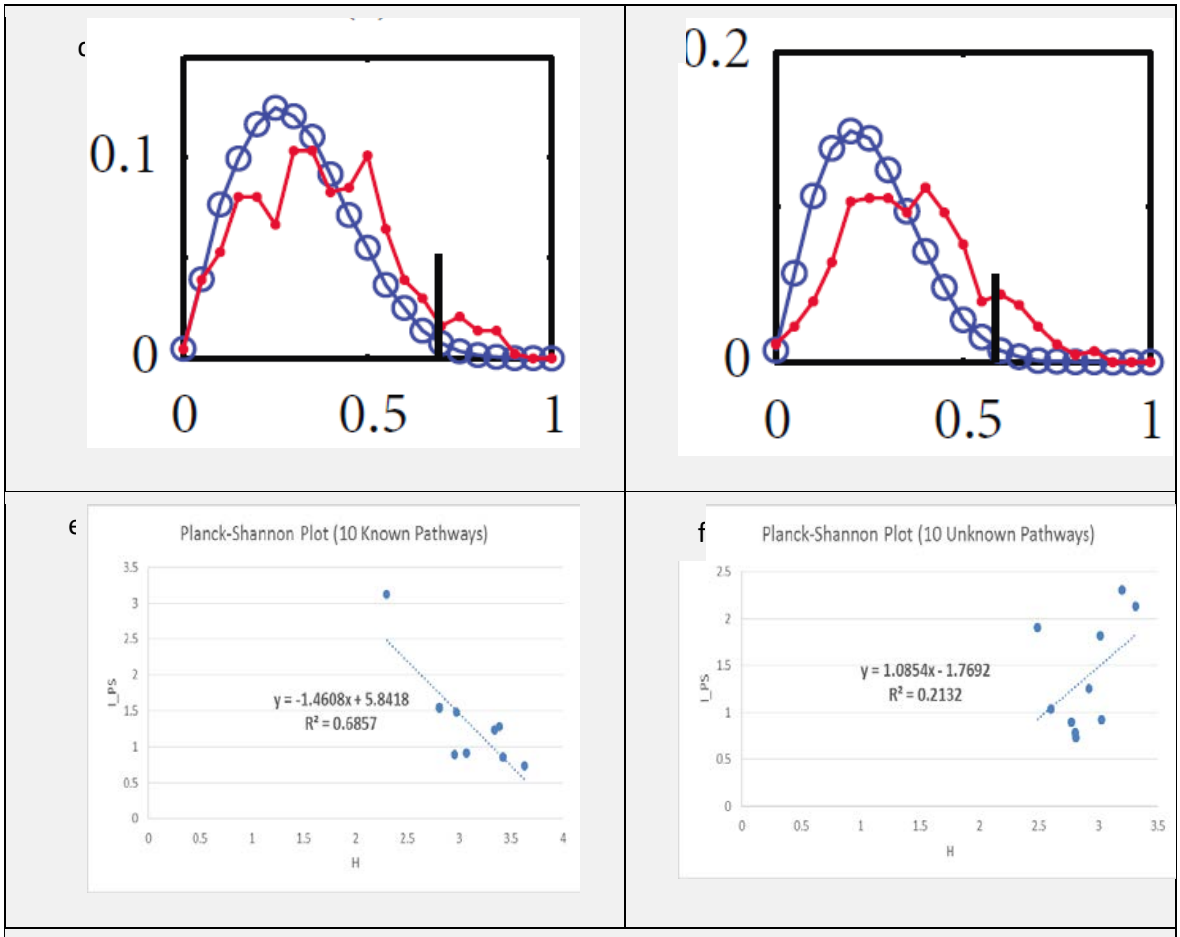

Figure 9. The multielectrode EEG measuring device as a tool to quantify consciousness based on the Planck-Shannon plot. (**a**) Multichannel EEG measuring device. (**b**) Local field potential (LFP) and Electroencephalograms (EEG) measured with multichannel EEG devices. **c**) & (d) The histograms of the phase synchronization indexes for original EEG signal pairs (red curves) and phase-shuffled surrogate pairs (blue curves) [20]. (**e**) The predicted appearances of the Planck-Shannon plots constructed from long-tailed histograms (such as shown in Panels **c** and d) measured from 10 different brain regions in conscious states. (f) Same as (**e**), except that the 10 brain regions are in unconscious state.

If one can measure EEG signals using two n-electrode EEG measuring devices, one placed on the cerebrum and the other on the cerebellum of a person and compute the I_{PS} and H values from the PDE's after fitting to these EEG data, one can obtain two Planck-Shannon plots from that person, each having n points

where n can be any number between say 3 and 100. I would predict that the more of the n points on the Plank-Shannon plot of the cerebrum would lie on a straight line than those on the Planck-Shannon plot of the cerebellum. If this prediction proves to be valid, one can assert that consciousness has a larger "superstructure" as measured by the Planck-Shannon plot than unconsciousness. It could also be predicted that the linearly correlated points on the Planck-Shannon plot of the cerebrum will be randomized to a greater extent that those points of the Planck-Shannon plots of the cerebellum upon administering an anesthetics to the person under study. The ratio between the degrees of randomization of these two points may be defined as the quantitative measure of consciousness (QMC). If the concept of QMC can be substantiated in the future, it my open up a new era in consciousness studies and divide the field into the *qualitative* and the *quantitative* consciousness studies. Finally, I am inclined to predict that QMC may exhibit the regional specificity in the cerebrum, i.e., QMC may be brain-region specific, a property which may make QMC a useful tool for mapping brain functions to brain dynamics.

In **Table 2** below, I compared the Planck-Shannon plot approaches to identifying superstructures in cell biology and consciousness studies. If the content of **Table 2** turns out to be valid upon further scrutiny, the Planck-Shannon plot may allow neuroscientists to identify and quantitatively study the brain regions that are responsible for the conscious state of the human mind, thus ushering in the new era of (what may be referred to as) the Quantitative Consciousness Study (QCS) or of the Quantum of Consciousness Study (QCS), in analogy to the Quantum of Action that initiated the era of Quantum Physics over a century ago.

Table 2. The Planck-Shannon approach to identifying superstructures in cell biology and consciousness studies.

	Cell Metabolism	**Consciousness Study**

Measuring device	Microarrays	Multichannel EEG devices
Data	mRNA levels in cells	Phase synchrony indexes in brains [20]
Structure	Metabolic pathways (or Metabolons [21])	*Phase synchronized neurons* within brain regions
Superstructure	Systems of correlated metabolic pathways (New drug targets)	*Phase synchronized neurons* between two or more remote brain regions (New brain regions supporting consciousnes)

Department of Pharmacology and Toxicology, Ernest Mario School of Pharmacy, Rutgers University, Piscataway, N.J.

REFERENCES:

[1] Ji, S. (2018). *The Cell Language Theory: Connecting Mind and Matter*. World Scientific Publishing, New Jersey.

[2] Ji, S. (1997). Isomorphism between cell and human languages: Molecular Biological, bioinformatics and linguistic implications. *BioSystems* **44**:17-39.

[3] Ji, S. (2019). The Molecular Linguistics of DNA: Letters, Words, Sentences, Texts, and their Meanings. In: *Theoretical Information Studies* (M. Burgin and G. Dodig-

Crnkovic, eds.), World Scientific Publishing (in press).

[4] Petoukhov, S. V. (2016). The system-resonance approach in modeling genetic structures. *Biosystems* **139**: 1-11.

[5] Trifonov, E. N. (1989). The multiple codes of nucleotide sequences. *Bull Math Biol.* **51**(4):417-32.

[6] Trifonov, E. N. (2008). Codes of biosequences". In *The Codes of Life.* ***1*** (Barbieri, M., ed.). Springer, pp. 3–14. ISBN 978-1-4020-6339-8.

[7] Norris, V. et al. (1999). Hypothesis: Hyperstructures regulate bacterial structure and the cell cycle. *Biochimie* **81:** 915-920.

[8] Ji, S. (2012). Molecular Theory of the Living Cell: Concepts, Molecular Mechanisms, and Biomedical Applications. Springer, New York.

[9] Lu, H. P., Xun, L. and Xie, X. S. (1998). Single-Molecule Enzymatic Dynamics. *Science* **282**: 1877-1882.

[10] Ji, S. (2015). Planckian distributions in molecular machines, living cells, and brains: The wave-particle duality in biomedical sciences. In: P*roceedings of the International Conference on Biology and Biomedical Engineering,* Vienna, March 15-17, 2015. Pp. 115-137.

[11] Blackbody radiation. http://hyperphysics.phy-astr.gsu.edu/hbase/mod6.html.

[12] Ji, S. (1991). Molecular Theories of Cell Life and Death. Rutgers University Press, New Brunswick. Pp. 177-178.

[13] Ratcliff, R. and McKoon, G. (2006). The Diffusion Decision Model. http://digitalunuion.osu.edu/r2/summer06/webb/index.html

[14] Luce, R.D. (1986) *Response Times: Their Role in Inferring Elementary Mental Organization.* New York: Oxford University Press. Figure 11.4.

[15] Deco, G., Rolls, E. T., Albantakis, L. and Romo, R. (2013) Brain mechanisms for perceptual and reward-related decision-making. *Progr Neurobiol* **103**: 194–213.

[16] Roxin, A. and Lederberg, A. (2008) Neurobiological Models of Two-choice Decision Making Can Be Reduced to a One-Dimensional Nonlinear Diffusion Equation. *PLoS Computational Biology* **4**(3): 1-13.

[17] Vandekerckhove, J., Tuerlinckx, F. (2007) Fitting the Ratcliff diffusion model to experimental data. *Psychonomic Bulletin & Review* **14**(6):1011-1026.

[18] Ji, S. (2018). Mathematical (Quantitative) and Cell Linguistic (Qualitative) Evidence for Hypermetabolic Pathways as Potential Drug Targets. *J. Mol. Gene. Med.* **12** (2): 1000343.

[19] Perou, C. M., Sorlie, T., Eisen, M. B., et al. (2000). Molecular portraits of human breast Tumors. Nature 406(6797): 747-52.

[20] Sun, J., Li, Z., and Tong, S. (2012). Inferring Functional Neural Connectivity with

Phase Synchronization Analysis: A Review of Methodology. Computational and Mathematical Methods in Medicine, Volume 2012, Article ID 239210, 13 pages doi:10.1155/2012/239210.

[21] Srere, P.A. (1987). Complexes of Sequential Metabolic Enzymes. Ann. Rev. Biochem. 56: 89-124.